

High-pressure elastic properties of the orientationally disordered and hydrogen-bonded phase of solid HCl

H. Shimizu, K. Kamabuchi, T. Kume, and S. Sasaki

Department of Electronics, Gifu University, 1-1 Yanagido, Gifu 501-1193, Japan
and CREST, Japan Science and Technology Corporation, Kawaguchi, Saitama 332-0012, Japan

(Received 22 July 1998; revised manuscript received 30 November 1998)

By using *in situ* Brillouin spectroscopy in a diamond-anvil cell, we have measured the direction-dependent acoustic velocities and the refractive index in the orientationally disordered and hydrogen-bonded solid phase I of hydrogen chloride (HCl) at pressures up to 4.5 GPa and 300 K, leading to the first determinations of adiabatic elastic constants (C_{11} , C_{12} , and C_{44}), bulk modulus (B_s), and the elastic anisotropy (A) to 4.5 GPa. These results are compared with those of solids of the same type H_2S and NH_3 . We investigate the effect of the strength of hydrogen bonds on the A value which is sensitive to the rotation-translation coupling of molecular motions under compression. [S0163-1829(99)01318-1]

I. INTRODUCTION

Raman and Brillouin scattering techniques with the diamond-anvil cell (DAC) are useful to study high-pressure optical and elastic properties of simple molecular solids, which are important to a wide range of problems in molecular and planetary sciences.¹ Raman scattering of crystalline solids at high pressure provides information about structural properties, phase transitions, and interatomic and intermolecular forces. High-pressure Brillouin scattering can be used to probe acoustic velocities, which yield the determinations of elastic constants, bulk modulus, the refractive index, and the equation of state of materials.²

Recently, we had developed high-pressure Brillouin spectroscopy for molecular single crystals grown in a DAC.^{3,4} A complete mapping of the acoustic velocities in the various crystal directions, the refractive index, and the full set of adiabatic elastic constants can be exactly determined with *in situ* identification of the crystal orientation at each pressure by analyzing the observed angular dependence of acoustic velocities. This elaborate method has been applied to an important group of simple molecular solid phase encountered first at room temperature with increasing pressure: H_2S ,^{3,5} CO_2 ,⁶ H_2O ,⁷⁻⁹ CH_4 ,¹⁰ Kr,¹¹ and NH_3 .¹² High-pressure studies of this group can explore a wide range of bond geometry and strength.

Our studied molecular solids are classified in Table I by having or not having the hydrogen bond and the molecular rotation, where solid HCl is the case of the present study. HCl, H_2S , and NH_3 solids show both the hydrogen bond and the molecular rotation in an orientationally disordered (OD) face-centered-cubic (fcc) phase, that is, in their plastic phase I, I, and III, respectively. As seen in Fig. 1(a), each HCl molecule has 12 equally probable equilibrium orientations, and random flips between these occur by the breaking and remaking of temporary hydrogen bonds. Solid CH_4 shows the typical fcc OD phase I above 1.6 GPa at 300 K, but it has no hydrogen bond at all and has a closed-shell spherical electronic configuration like rare-gas solids [see Fig. 1(b)]. The rare-gas solid Kr has a fcc structure at pressures above 0.83 GPa at 300 K, and does not contain rotating molecules [see Fig. 1(c)]. Therefore solid Kr can be regarded as a standard

crystal for studying fcc molecular solids.

In this paper, we present the first results of *in situ* Brillouin scattering in solid phase I of hydrogen chloride HCl at pressures up to 4.5 GPa and 300 K, and determine the pressure dependence of acoustic velocities for all directions, the refractive index, the density, adiabatic elastic constants (C_{11} , C_{12} , and C_{44}), adiabatic bulk modulus (B_s), and the elastic anisotropy [$A = 2C_{44}/(C_{11} - C_{12})$]. These results of one Cl-H bonded HCl are compared with our previous results of two S-H bonded H_2S (Refs. 3 and 5) and three N-H bonded NH_3 .¹² Furthermore, from a point of view presented in Table I and Fig. 1, we will investigate the effect of hydrogen bonds on the molecular rotation and on the elasticity, in particular on the elastic anisotropy which is sensitive to the rotation-translation (RT) coupling of molecular motions under compression.¹⁰

II. EXPERIMENT AND ANALYSIS

For loading a HCl sample in a DAC, we condensed commercial gaseous HCl (purity, 99.999%) by spraying its vapor into the gasket hole (diameter 0.2 mm, depth 0.2 mm) of the DAC cooled in a liquid-nitrogen bath. When the hole was full of solidified HCl, the upper diamond was translated to seal the sample. To avoid the contamination into the sample, the above procedure was carried out in the nitrogen atmosphere. After adequate pressure had been applied, the DAC

TABLE I. Classification of pressure-induced cubic molecular solids at 300 K by having (○) or not having (×) the hydrogen bond and the molecular rotation.

Simple molecular solids	Hydrogen bond	Molecular rotation	Type
HCl, H_2S , NH_3	○	○	(1)
H_2O	○	×	(2)
CH_4	×	○	(3)
Kr	×	×	(4)
CO_2	×	×	(4)

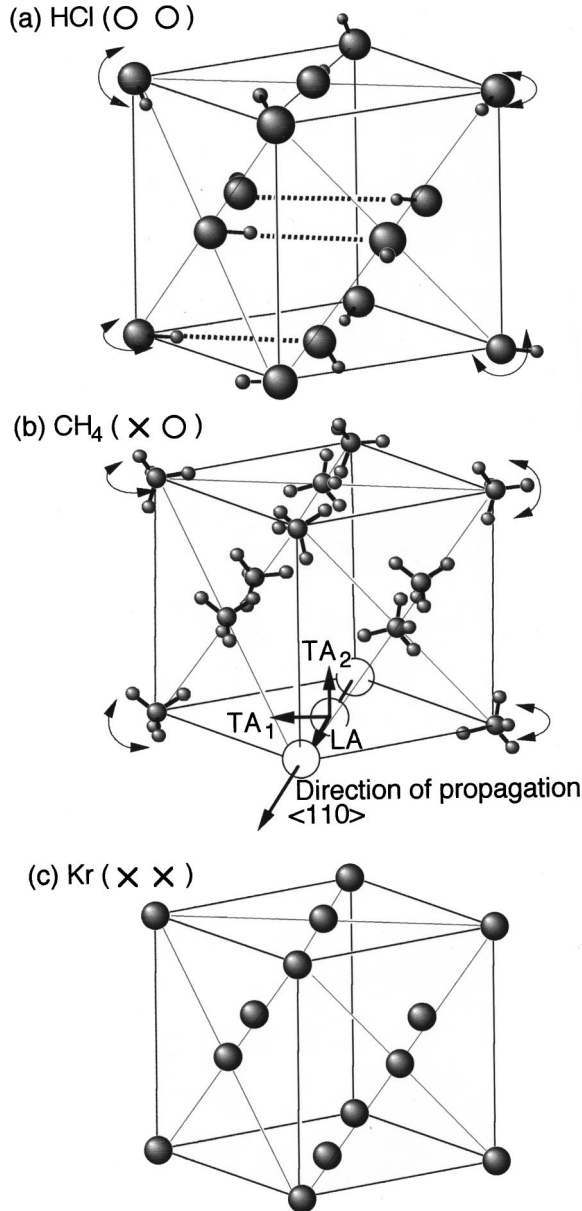


FIG. 1. Pressure-induced fcc crystal structures of (a) HCl (phase I), (b) CH₄ (phase I), and (c) Kr at 300 K. Solid HCl shows both the hydrogen band and the molecular rotation (O O), and solid CH₄ shows only the molecular rotation (XO). (b) CH₄, the directions of polarization for a LA and two TA modes propagating along $\langle 110 \rangle$ direction are shown to define the elastic anisotropy $A = (v_{TA_2}/v_{TA_1})^2 = 2C_{44}/(C_{11} - C_{12})$.

was warmed to room temperature.⁴ A single crystal of HCl was grown by increasing the pressure on a seed crystal, which coexists with the liquid at 0.7 GPa. No pressure transmitting medium was used. The pressure was measured by the ruby-scale method.

For Brillouin measurements, the 514.5 nm argon-ion laser line (λ_0) with a single longitudinal mode was used with an input power level of about 100 mW. The heart of the apparatus was a Sandercock tandem Fabry-Perot interferometer,¹³ which was used in a triple-pass arrangement. The Brillouin frequency shifts ($\Delta\nu$) at 60°, 90°, and 180° scattering geometries with the DAC (angles between incident and scattered beams) are related to the acoustic velocity (v) as follows:²

$$\Delta\nu_{60} = v_{60}/\lambda_0, \quad (1)$$

$$\Delta\nu_{90} = \sqrt{2}v_{90}/\lambda_0, \quad (2)$$

and

$$\Delta\nu_{180} = (2n)v_{180}/\lambda_0, \quad (3)$$

where the wave vector \mathbf{q} of the acoustic phonons is parallel (60° and 90°) and perpendicular (180°) to the interfaces of the input and output diamonds crossed by the laser beam, and v_{60} and v_{90} are independent of the refractive index (n) of the medium. By using Eq. (3), we can determine the refractive index, because $\Delta\nu_{180}$ is measured, and v_{180} is calculated by our *in situ* Brillouin scattering method described next.

From the Brillouin equation for the cubic system, Every¹⁴ derived the relation between sound velocities for arbitrary directions and elastic constants (C_{11} , C_{12} , C_{44}). The ρv_j^2 is expressed as a function of six parameters as follows:

$$\rho v_j^2 = f_j(C_{11}, C_{12}, C_{44}, q_x, q_y, q_z), \quad (4)$$

where ρ is density, subscript j ($=0, 1, 2$) indicates LA, TA₁ (slow), and TA₂ (fast) modes, respectively, and q_x , q_y , and q_z are direction cosines of the phonon. For the application of these results to our experimental system, we set up the geometrical relation of Cartesian coordinates: Euler angles (θ , ϕ , χ) relate the laboratory frame (X, Y, Z) to the crystal reference frame (x, y, z). The v_j therefore can be expressed as a function of six parameters:

$$v_j = g_j(C_{11}/\rho, C_{12}/\rho, C_{44}/\rho, \theta, \phi, \chi), \quad (5)$$

where $q_x = \cos\theta \cos\phi \cos\chi - \sin\phi \sin\chi$, $q_y = -\cos\theta \cos\phi \sin\chi - \sin\phi \cos\chi$, and $q_z = \sin\theta \cos\phi$. In order to determine three Euler angles and three elastic constants at each pressure, we measured the Brillouin frequency shifts at 60° or 90° scattering geometry at 10° intervals of the rotation angle ϕ about the load axis of the DAC. Next, we applied a computerized least-squares fit between calculations $g_j(\phi_i)$ and experimental velocities (ϕ_i , v_{ji}) as a function of angle ϕ_i :

$$J = \sum_{ij} [g_j(\phi_i) - v_{ji}]^2, \quad j=0,1,2, \quad (6)$$

where J is minimized by systematically varying the six parameters until the fit is optimized. As a result, we can determine acoustic velocities for all directions with *in situ* identification of the crystal orientation (θ , ϕ , χ) at each pressure.

III. RESULTS AND DISCUSSION

We have determined the pressure dependence of the acoustic velocities, the refractive index, the density, the polarizability, adiabatic elastic constants, bulk modulus, and the elastic anisotropy in HCl solid phase I (Ref. 15) at pressures up to 4.5 GPa and 300 K. These results are compared with our previous results for H₂S, NH₃, and other simple molecular solids.

A. Acoustic velocity

Figure 2 shows a typical Brillouin spectrum of solid HCl at 2.44 GPa. The longitudinal (LA) and two transverse (TA₁, TA₂) modes are clearly observed. Brillouin measurements at

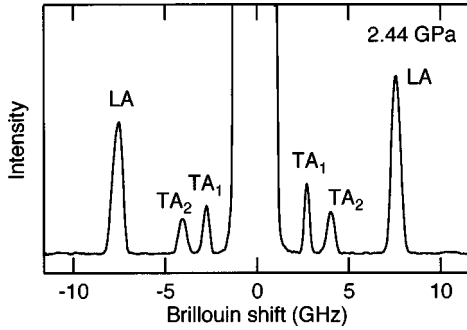


FIG. 2. Brillouin spectrum of solid HCl at $P=2.44$ GPa. Scattering angle is 60° . LA, TA_2 , and TA_1 are Brillouin-shifted signals from longitudinal, fast, and slow transverse modes, respectively.

60° scattering geometry were made at 10° intervals of rotation angle ϕ about the load axis of the DAC in the laboratory frame. The observed Brillouin frequency shifts, that is, acoustic velocities at 2.44 GPa, are plotted as a function of ϕ as open circles in Fig. 3. To analyze the angular dependence of the acoustic velocities for the LA, TA_1 , and TA_2 modes, we used Eqs. (5) and (6). We found excellent agreement between the measured and the fitted values, as seen in Fig. 3, which yielded $C_{11}/\rho = 11.40 \pm 0.02$, $C_{12}/\rho = 8.12 \pm 0.02$, and $C_{44}/\rho = 4.96 \pm 0.01 \text{ km}^2/\text{s}^2$, and the crystal orientation in the DAC ($\theta = 30.4 \pm 0.2^\circ$ and $\chi = 66.1 \pm 0.1^\circ$ at 2.44 GPa). Figure 4 shows the pressure dependence of C_{ij}/ρ determined for liquid (up to 0.7 GPa) and solid HCl at room temperature. The square of bulk sound velocity, $v_B^2 = [(C_{11} + 2C_{12})/(3\rho)]$ is also presented by a dotted line.

Once the six parameters were determined, the acoustic velocities could be calculated for all directions. In Figs. 5(a) and 5(b), the HCl sound velocities of solid phase I are shown respectively for $\langle 100 \rangle$ and $\langle 110 \rangle$ directions as a function of pressure up to 4.5 GPa at 300 K, and our previous results of the H_2S (phase I) and NH_3 (phase III) velocities are also presented for comparisons. All LA and TA velocities in their OD phases of HCl, H_2S , and NH_3 solids show almost the same pressure dependence, but their values of acoustic velocities are different. To compare these sound velocities, we show the pressure dependence of bulk sound velocity for HCl, H_2S , and NH_3 solids in Fig. 5(c); for example, at P

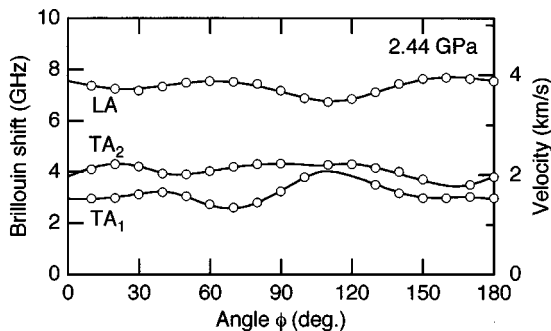


FIG. 3. Brillouin frequency shifts and acoustic velocities of LA, TA_2 , and TA_1 modes as a function of angle ϕ at a 60° scattering geometry for solid HCl at $P=2.44$ GPa. The ϕ shows the rotation angle about the load axis of DAC. Open circles indicate experimental points, and the solid lines represent the calculated best-fit velocities.

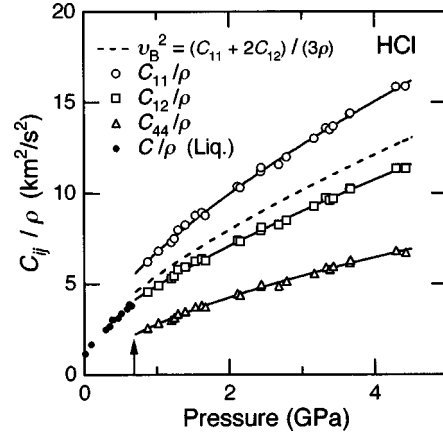


FIG. 4. Pressure dependence of C_{ij}/ρ for liquid HCl (solid circles) and solid HCl (open symbols) at room temperature. The square of bulk sound velocity, $(C_{11} + 2C_{12})/(3\rho)$ is represented by dotted line. Vertical arrow indicates the liquid-solid phase-transition point at $P=0.7$ GPa.

$=3.0$ GPa they indicate $v_B = 3.20$, 3.48, and 4.44 km/s, respectively. Molecular kinetic theory suggests that $v_{B-\text{HCl}}:v_{B-\text{H}_2\text{S}}:v_{B-\text{NH}_3} \approx 1/\sqrt{M_{\text{HCl}}}:1/\sqrt{M_{\text{H}_2\text{S}}}:1/\sqrt{M_{\text{NH}_3}} = 1.0:1.03:1.46$, where M_{HCl} , $M_{\text{H}_2\text{S}}$, and M_{NH_3} are the molecular weights of HCl ($=36.46$), H_2S ($=34.08$), and NH_3 ($=17.03$) respectively. The present experimental results of v_B are 1.0: 1.08: 1.39, which seems to be in fair agreement with the above calculations.

B. Refractive index, density, and polarizability

The determination of C_{ij}/ρ was systematically carried out in HCl phase I at pressures between 0.7 and 4.5 GPa. Therefore we can calculate the acoustic velocity (v_{180}) along the direction perpendicular to the diamond interfaces, which is available to determine the refractive index (n) by using Eq. (3). From the Δv_{180} measured at 180° scattering geometry, we can obtain the pressure dependence of n for solid HCl as shown by the open circles in Fig. 6. We also show the pressure dependence of n in HCl liquid phase below 0.7 GPa at room temperature by solid circles. The refractive index is almost continuous across the freezing point at 0.7 GPa, and shows a gradual increase with pressure from $n=1.51$ at 1.02 GPa to $n=1.67$ at 4.43 GPa. The result for solid HCl is compared with our previous results for H_2S and NH_3 solids in the inset of Fig. 6; the refractive index of solid H_2S shows higher values than HCl and NH_3 solids at all pressures.

From the refractive index (n) determined at each pressure, we can estimate the polarizability (α) by the use of the Lorentz-Lorenz equation:

$$\frac{n^2 - 1}{n^2 + 2} = \frac{4}{3} \pi \alpha \frac{N\rho}{M} = \frac{4}{3} \pi \alpha \frac{N}{V}, \quad (7)$$

where N , ρ , M , and V are Avogadro's number, density, molecular weight, and molar volume, respectively. Then, we need the pressure dependence of ρ for solid HCl in the pressure range studied here, however, no one has the experimental data except for the x-ray-diffraction data determined recently by Fujihisa *et al.*¹⁶ in higher pressure range between

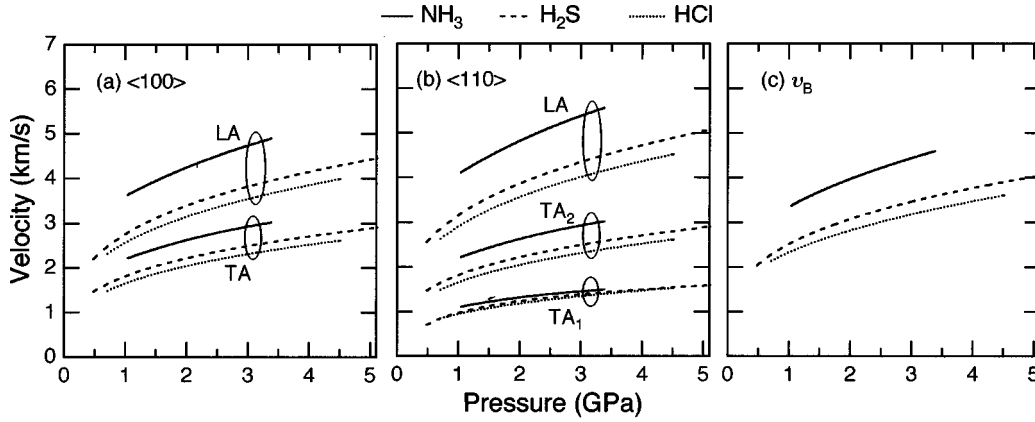


FIG. 5. Pressure dependence of sound velocities for HCl, H₂S, and NH₃ solids at 300 K along (a) $\langle 100 \rangle$ and (b) $\langle 110 \rangle$ direction. The bulk sound velocities (v_B) are also shown as a function of pressure.

10.6 and 28 GPa at ambient temperature; for example, $\rho = 2.44, 2.66,$ and 2.82 g/cm^3 at $P = 10.6, 15.8,$ and 20.3 GPa , respectively. Therefore we extrapolated their data to our pressure range by the use of a fit of Birch-Murnaghan equation:^{17,18}

$$P = \left(\frac{3}{2}\right)B_0(y^7 - y^5)\left[1 - \left(\frac{3}{4}\right)(4 - B'_0)(y^2 - 1)\right], \quad (8)$$

where B_0 is the bulk modulus at zero (atmospheric) pressure, B'_0 the pressure derivative of the bulk modulus, $y = (\rho/\rho_0)^{1/3}$ with ρ_0 the density at zero pressure and ρ the density at pressure P . Usually, B_0 , B'_0 , and ρ_0 are the fitting parameters. In this case, however, the value of ρ_0 should be set because of the lack of experimental data in the low-pressure range.

The value of ρ_0 was estimated as follows. In the previous studies, the zero-pressure densities at low temperatures were determined; $\rho_0 = 1.441 \text{ g/cm}^3$ at 130 K (Ref. 18) and $\rho_0 = 1.470 \text{ g/cm}^3$ at 118.5 K.¹⁹ Although only the two data are not sufficient for the extrapolation to room temperature, ρ_0 was roughly estimated to be 1.1 g/cm^3 at 300 K by the linear extrapolation for the molar volume. Next, we varied ρ_0 around 1.1 g/cm^3 , i.e., from $0.9\text{--}1.3 \text{ g/cm}^3$, and obtained the various fitted curves of ρ as a function of pressure. The $\rho(P)$ gives rise to the P dependence of the specific heat ratio [$\gamma \equiv C_p/C_v = B_S/B_T$] by using the present data [$v_B^2 = (C_{11} + 2C_{12})/(3\rho)$] and the relation of $\gamma = v_B^2 d\rho/dP$. The obtained $\gamma(P)$ was sensitive to ρ_0 . If ρ_0 is set to 1.3 or more, γ increases with increasing pressure in the low-pressure region, which is inconsistent with the general behavior of $\gamma(P)$ showing the decrease with pressure.^{2,4,11,12} If ρ_0 is set to 0.9 or less, the value of γ becomes 1.41 or more at 0.87 GPa, which may be too large considering $\gamma = 1.41$ for gaseous HCl.²⁰ Therefore the values of ρ_0 from $0.9\text{--}1.3 \text{ g/cm}^3$ seem to be plausible. Even if the set value of ρ_0 is varied from $0.9\text{--}1.3 \text{ g/cm}^3$, the fitted curve of $\rho(P)$ was fluctuated within $\pm 5\%$ in the pressure range studied here. Therefore we used $\rho_0 = 1.1 \text{ g/cm}^3$ for the determination of the equation of state (EOS). The conclusive EOS of solid HCl up to 20 GPa is as follows:

$$P = \left(\frac{3}{2}\right)B_0\left[\left(\frac{\rho}{1.1}\right)^{7/3} - \left(\frac{\rho}{1.1}\right)^{5/3}\right]\left\{1 - \left(\frac{3}{4}\right)(4 - B'_0)\right. \\ \left. \times \left[\left(\frac{\rho}{1.1}\right)^{2/3} - 1\right]\right\}, \quad (9)$$

where $B_0 = 0.793 \pm 0.18 \text{ GPa}$ and $B'_0 = 8.62 \pm 1.37$, P in GPa and ρ in g/cm^3 . By using the $n(P)$ of solid HCl in Fig. 6, and Eqs. (7) and (9), we could determine the pressure dependence of the polarizability; α shows its value of $2.79 \times 10^{-24} \text{ cm}^3$ at 1.5 GPa and gradually decreases with pressure to $2.69 \times 10^{-24} \text{ cm}^3$ at 4.5 GPa.

Next, let us compare the present result of solid HCl with the previous results^{3,5,12} of H₂S and NH₃, to estimate their refractive indices shown in the inset of Fig. 6. We note here typical parameter values at $P = 3.0 \text{ GPa}$: n ; 1.63, 1.80, 1.57, ρ ; 1.86, 1.53, 1.05 g/cm^3 , V ; 32.6, 37.0, 26.9 \AA^3 , α ; 2.76×10^{-24} , 3.78×10^{-24} , $2.10 \times 10^{-24} \text{ cm}^3$, for solid HCl, H₂S, and NH₃, respectively. It has turned out from Eq. (7) that higher values of n for solid H₂S (see Fig. 6) are originated from larger values of polarizability in H₂S solid phase I.

C. Adiabatic elastic constant and bulk modulus

The EOS of Eq. (9) yielded the first determination of three adiabatic elastic constants of solid HCl by the use of C_{11}/ρ , C_{12}/ρ , and C_{44}/ρ in Fig. 4. Their pressure dependence of C_{ij} and of the adiabatic bulk modulus (B_S) are

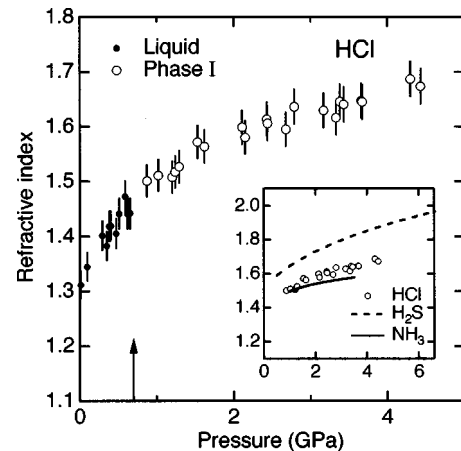


FIG. 6. Pressure dependence of the refractive indices (n) for liquid HCl (solid circles) and solid phase I of HCl (open circles) at 300 K. Vertical arrow indicates the liquid-solid phase transition point at $P = 0.7 \text{ GPa}$. The inset shows the comparison of n among HCl, H₂S, and NH₃ solids.

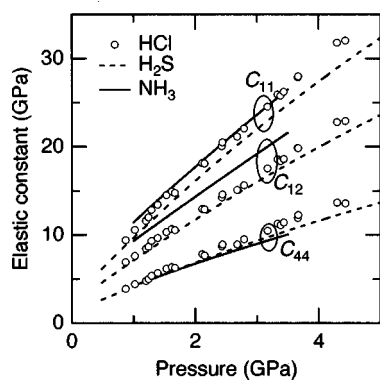


FIG. 7. Pressure dependence of adiabatic elastic constants C_{11} , C_{12} , and C_{44} for HCl, H_2S , and NH_3 solids at 300 K.

shown as open circles in Figs. 7 and 8, respectively. All the elastic constants and bulk moduli are found to increase almost linearly with pressure. Typical values for solid HCl were $C_{11}=22.1$, $C_{12}=15.6$, and $C_{44}=9.51$ GPa, and $B_S = 17.8$ GPa at $P=2.79$ GPa. Taking account of the uncertainties in ρ which were approximately $\pm 5\%$, the relative accuracies on C_{ij} are about $\pm 6\%$. The results of C_{ij} and B_S in H_2S solid phase I and NH_3 solid phase III are also shown as dotted and solid lines in Figs. 7 and 8, respectively. Except for C_{12} of solid NH_3 , three C_{ij} show respectively close values at each pressure. C_{12} of solid NH_3 shows a larger value close to C_{11} at all pressure, which is reflected on a larger B_S and the high degree of the elastic anisotropy A as reported next.

D. Elastic anisotropy

Although the fcc crystals are optically isotropic, they exhibit substantial elastic anisotropy (A) which is defined as follows:²¹

$$A = (v_{TA_2}/v_{TA_1})^2 = 2C_{44}/(C_{11} - C_{12}), \quad (10)$$

where v_{TA_2} and v_{TA_1} are, respectively, sound velocities of the TA_2 and TA_1 modes propagating along $\langle 110 \rangle$ directions. This system is shown for the case of solid CH_4 in Fig. 1(b). For isotropic elasticity, the two shear velocities v_{TA_2} and v_{TA_1} are equal and $A = 1$.

For fcc solids showing molecular rotation in their OD phase, the elastic anisotropy has been the subject of numerous experimental and theoretical investigations regarding

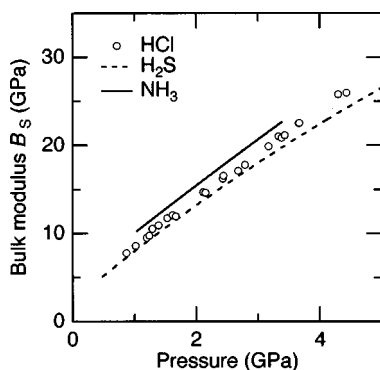


FIG. 8. Pressure dependence of adiabatic bulk moduli (B_S) for HCl, H_2S , and NH_3 solids at 300 K.

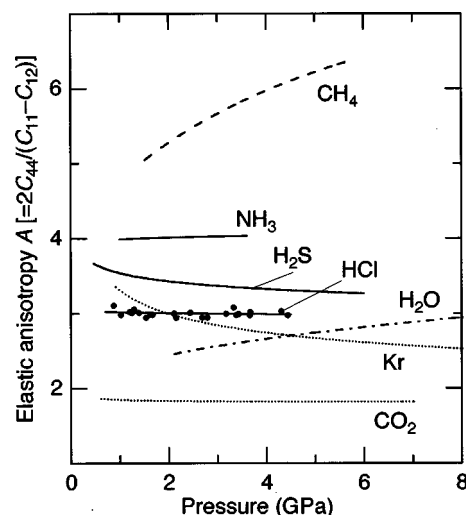


FIG. 9. Pressure dependence of elastic anisotropy [$A = 2C_{44}/(C_{11} - C_{12})$] for pressure-induced cubic solids CH_4 , NH_3 , H_2S , HCl, H_2O , Kr, and CO_2 at 300 K.

the rotation-translation (RT) coupling of molecular motions. Typical example is the case of solid CH_4 : Rand and Stoicheff²¹ found that the velocity of the TA_1 mode is anomalously low, i.e., strong damping occurs in the $\langle 110 \rangle$ direction [see Fig. 1(b)]. Therefore large value of A is indicative of significant RT coupling of molecules. This effect of RT coupling was confirmed theoretically by Wonneberger and Hüller.²² Recently, we have found the remarkable increase of A with pressure for solid CH_4 (Ref. 10) as shown in Fig. 9. This pressure effect indicates that the coupling of molecular rotations with the TA_1 mode is strong, and becomes stronger with increasing pressure, effectively along $\langle 110 \rangle$ direction of the fcc solid CH_4 .

Our present purpose is to investigate the effect of hydrogen bonds on the molecular rotation, that is, on the RT coupling for HCl, H_2S , and NH_3 solids which show both the hydrogen bond and the molecular rotation in their OD phase. Figure 9 shows the pressure dependence of the elastic anisotropy A for simple molecular solids listed in Table I. Most molecular solids like CO_2 show $A \cong 2$ and almost independent on pressure. Solid CH_4 presents the anomalous feature of A increasing with pressure, as mentioned before, which is caused by the increasing RT coupling in the OD phase I.¹⁰ On the other hand, the rare-gas solid Kr with no molecular rotation exhibits $A = 3.3$ at $P = 1$ GPa, and shows a gradual decrease with increasing pressure.¹¹ These differences in A values between solid CH_4 and Kr mean that a significant contribution comes from the effect of RT coupling. Solid HCl shows the smallest $A = 3$ at $P = 1$ GPa among HCl, H_2S , and NH_3 solids, and its A decreases a little against pressure. The A value of solid H_2S exists in a middle region, and decreases gradually with pressure. Solid NH_3 shows a large A value of about 4, which is almost independent of pressure. These features of hydrogen-bonded and OD solids are in marked contrast to that of OD solid CH_4 . The role of the hydrogen bond in this system can be considered as shown schematically in Fig. 10, as an example, for the case of H_2S ; each H_2S molecule shows random flips between their equilibrium orientations by the breaking and remaking of temporary hydrogen bonds. By increasing pressure the strength of

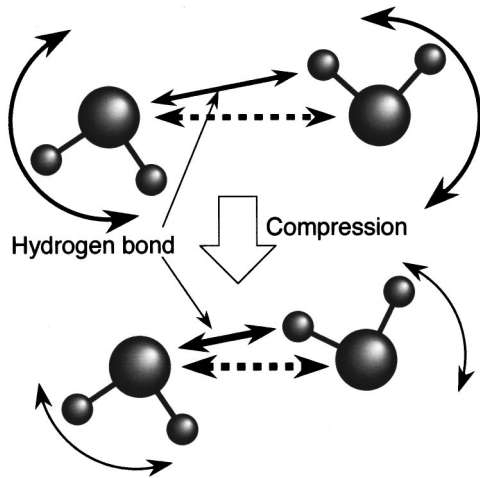


FIG. 10. Image of the depression of molecular rotation (H_2S) due to the increasing strength of the hydrogen bond under compression.

hydrogen bond becomes strong, as a result, the molecular rotations are depressed. Therefore we can propose two factors which dominate the value of A . One is the RT coupling which increases A , and the other is the strength of hydrogen bond which decreases A . For the A value of solid NH_3 , which is independent of pressure, the former and the latter are considered to balance against applied pressure. To investigate the strength of hydrogen bond under high pressure, we can list up the pressure dependence of the intramolecular stretching frequency (ν_1) reported previously; $d\nu_1/dP = -29 \text{ cm}^{-1}/\text{GPa}$ for HCl ,²³ $d\nu_1/dP = -10.1 \text{ cm}^{-1}/\text{GPa}$ for H_2S ,²⁴ and $d\nu_1/dP = -6.1 \text{ cm}^{-1}/\text{GPa}$ for NH_3 .²⁵ These negative values indicate the degree of increasing strength of hydrogen bond against applied pressure. Therefore the degree of the increasing strength of hydrogen bond under com-

pression can be formed in order of HCl , H_2S , and NH_3 . As a result, strongly depressed RT coupling yielded lower A value for HCl , and fairly depressed RT coupling determined the medium value for H_2S , and also high value for NH_3 .

As for VII phase (bcc) of H_2O ice (see Table I), the value of A is small because of no molecular rotation. With increasing pressure the elastic anisotropy A increases gradually as seen in Fig. 9. This is the structural consequence of the increasing strength of hydrogen bond under compression. At higher pressures around 8 GPa, the A values of H_2O , HCl , and H_2S seem to get together, which suggests that the molecular rotation becomes weak (or disappears) and the hydrogen bond dominates the elastic anisotropy for HCl and H_2S solids. In case of this investigation for solid NH_3 , we need more information of elastic properties in another phase IV above 3.5 GPa.

IV. CONCLUSION

By using *in situ* Brillouin spectroscopy, we determined the direction-dependent acoustic velocities and the refractive index for solid phase I of HCl as a function of pressure up to 4.5 GPa and 300 K. Our fitted Birch-Murnaghan EOS for solid HCl yielded determinations of adiabatic elastic constants C_{11} , C_{12} , and C_{44} , and adiabatic bulk modulus B_S at pressures up to 4.5 GPa and 300 K. These results for solid HCl were compared with the same type H_2S and NH_3 solids showing the hydrogen bond and the molecular rotation.

We presented the pressure dependence of the elastic anisotropy A for cubic molecular solids HCl , H_2S , NH_3 , H_2O , CH_4 , Kr , and CO_2 . To investigate these behaviors of $A(P)$, we proposed two key factors: (1) the rotation-translation coupling which increases A , and (2) the strength of hydrogen bond which decreases A . This gives us the systematic understanding for the elasticity of cubic molecular solids and their classification.

¹R. J. Hemley, P. M. Bell, and H. K. Mao, *Science* **237**, 605 (1987).

²H. Shimizu, E. M. Brody, H. K. Mao, and P. M. Bell, *Phys. Rev. Lett.* **47**, 128 (1981).

³H. Shimizu and S. Sasaki, *Science* **257**, 514 (1992).

⁴H. Shimizu, in *High Pressure Research on Solids*, edited by M. Senoo, K. Suito, T. Kobayashi, and H. Kubota (Elsevier, Netherlands, 1995), pp. 1–17.

⁵S. Sasaki and H. Shimizu, *J. Phys. Soc. Jpn.* **64**, 3309 (1995).

⁶H. Shimizu, T. Kitagawa, and S. Sasaki, *Phys. Rev. B* **47**, 11 567 (1993).

⁷H. Shimizu, M. Ohnishi, S. Sasaki, and Y. Ishibashi, *Phys. Rev. Lett.* **74**, 2820 (1995).

⁸H. Shimizu, T. Nabetani, T. Nishiba, and S. Sasaki, *Phys. Rev. B* **53**, 6107 (1996).

⁹H. Shimizu, *Rev. High Pressure Sci. Technol.* **7**, 1124 (1998).

¹⁰H. Shimizu, N. Nakashima, and S. Sasaki, *Phys. Rev. B* **53**, 111 (1996).

¹¹H. Shimizu, N. Saitoh, and S. Sasaki, *Phys. Rev. B* **57**, 230 (1998).

¹²T. Kume, M. Daimon, S. Sasaki, and H. Shimizu, *Phys. Rev. B* **57**, 13 347 (1998).

¹³R. Mock, B. Hillebrands, and R. Sandercock, *J. Phys. E* **20**, 656 (1987).

¹⁴A. G. Every, *Phys. Rev. Lett.* **42**, 1065 (1979).

¹⁵T. Kume, T. Tsuji, K. Kamabuchi, S. Sasaki, and H. Shimizu, *Proceedings of the 6th Japan-CIS/Baltic Symposium on Ferroelectricity*, Noda, Japan 1998 [*Ferroelectrics* **219**, 101 (1998)].

By the high-pressure Raman spectroscopy, it has been found that the pressure-induced solid HCl at 300 K shows the phase transitions of I(cubic)→I'(cubic) and I'→III(orthorhombic) at 4.5 and 17.0 GPa, respectively.

¹⁶H. Fujihisa and K. Aoki (private communication).

¹⁷F. Birch, *J. Geophys. Res.* **56**, 227 (1952).

¹⁸J. W. Stewart, *J. Chem. Phys.* **36**, 400 (1962).

¹⁹E. Sandor and R. F. C. Farrow, *Nature (London)* **213**, 171 (1967).

²⁰*Lange's Handbook of Chemistry*, edited by J. A. Dean (McGraw-Hill, New York 1973).

²¹S. C. Rand and B. P. Stoicheff, *Can. J. Phys.* **60**, 287 (1982).

²²S. Wonneberger and A. Hüller, *Z. Phys. B* **66**, 191 (1987).

²³P. G. Johannsen, W. Helle, and W. B. Holzapfel, *J. Phys. (Paris), Colloq.* **45**, C8, 199 (1984).

²⁴H. Shimizu, Y. Nakamichi, and S. Sasaki, *J. Chem. Phys.* **95**, 2036 (1991).

²⁵M. Gauthier, Ph. Pruzan, J. C. Chervin, and J. M. Besson, *Phys. Rev. B* **37**, 2102 (1988).